Chemistry of *C*-Trimethylsilyl-Substituted Main-Group Heterocarboranes. 6. Lead(II)-Inserted η^5-*closo*-Plumbacarboranes and Their Reactivity toward a Bidentate Lewis Base: Crystal Structures of *closo*-1-Pb-2-($SiMe_3$)-3-(R)-2,3-$C_2B_4H_4$ and 1-Pb($C_{10}H_8N_2$)-2,3-($SiMe_3$)$_2$-2,3-$C_2B_4H_4$ (R = $SiMe_3$, Me)

Narayan S. Hosmane,* Kai-Juan Lu, Hong Zhu, Upali Siriwardane, Manjunath S. Shet, and John A. Maguire

Department of Chemistry, Southern Methodist University, Dallas, Texas 75275

Received July 31, 1989

The monosodium salts of the carborane anions [2,3-($SiMe_3$)$_2$-2,3-$C_2B_4H_5$]$^-$, [2-($SiMe_3$)-3-(Me)-2,3-$C_2B_4H_5$]$^-$, and [2-($SiMe_3$)-2,3-$C_2B_4H_6$]$^-$ react with $PbCl_2$ to produce the corresponding *closo*-plumbacarboranes, 1-Pb-2,3-($SiMe_3$)$_2$-2,3-$C_2B_4H_4$ (I), 1-Pb-2-($SiMe_3$)-3-(Me)-2,3-$C_2B_4H_4$ (II), and 1-Pb-2-($SiMe_3$)-2,3-$C_2B_4H_5$ (III) in 25–37% yields. The plumbacarboranes I, II, and III were characterized on the basis of ^1H, ^{11}B, and ^{13}C pulse Fourier transform NMR, IR, and mass spectroscopy. Crystal structures of I and II show dimers of PbC_2B_4 cages arranged in layered networks. In I the dimers consist of identical molecules, while in II each dimer consists of two crystallographically independent molecules. Both I and II crystallized in the triclinic space group $P\bar{1}$ with a = 6.409 (6) and 6.343 (2) Å, b = 10.068 (11) and 12.286 (5) Å, c = 14.86 (2) and 16.593 (6) Å, α = 79.5 (1), and 73.33 (3)°, β = 88.3 (1) and 82.45 (3)°, γ = 74.13 (9) and 80.08 (3)°, U = 907 (2) and 1215.5 (8) Å^3, and Z = 2 and 2, respectively. Full-matrix least-squares refinements of I and II converged at R = 0.048 and 0.038 and R_w = 0.050 and 0.053, respectively. The *closo*-plumbacarboranes I, II, and III slowly form the donor–acceptor complexes 1-Pb($C_{10}H_8N_2$)-2,3-($SiMe_3$)$_2$-2,3-$C_2B_4H_4$ (IV), 1-Pb($C_{10}H_8N_2$)-2-($SiMe_3$)-3-(Me)-2,3-$C_2B_4H_4$ (V), and 1-Pb($C_{10}H_8N_2$)-2-($SiMe_3$)-2,3-$C_2B_4H_5$ (VI) with 2,2′-bipyridine in yields ranging from 61 to 84%. The complexes were characterized by ^1H, ^{11}B, and ^{13}C NMR, IR, and mass spectroscopy, and IV was also characterized by single-crystal X-ray diffraction. The crystal structure of IV showed a significant displacement of the apical lead from the centroidal position above the C_2B_3 face in a distorted pentagonal–bipyramidal geometry. The Pb-bound 2,2′-bipyridine base is not situated exactly opposite the C–C_{cage} bond; rather, it is tilted toward the two basal borons above the C_2B_3 face. Compound IV crystallized in the monoclinic space group $P2_1/n$ with a = 6.966 (4) Å, b = 35.49 (3) Å, c = 9.762 (8) Å, β = 102.30 (6)°, U = 2358 (3) Å^3, and Z = 4. Full-matrix least-squares refinement converged at R = 0.034 and R_w = 0.040.

Introduction

Research in the area of group 14 heterocarboranes, particularly of the MC_2B_4 system, has been quite active in recent years.[1] All elements in that group have been inserted into carborane cages, and in some cases, the insertions of the heteroatoms have been accomplished in both their +2 and +4 oxidation states. A great deal of structural information is available on several *closo*-stannacarboranes, *closo*-germacarboranes, and their donor–acceptor complexes, *commo*-germacarboranes and *commo*-silacarboranes.[1e,f] The least studied are the plumbacarboranes. The first example of an icosahedral plumbacarborane was reported by Rudolph et al. in 1970 as a member of the series *closo*-$MC_2B_9H_{11}$ (M = Ge, Sn, and Pb).[2] The smaller cage pentagonal bipyramidal plumbacarboranes of the type *closo*-1-Pb-2,3-(R)$_2$-2,3-$C_2B_4H_4$ (R = Me, H) were reported somewhat later by Wong and Grimes.[3] However, the solid-state structures of these compounds have not been reported. In our recent preliminary communication, we have confirmed, through the X-ray crystal structure of 1-Pb-2,3-($SiMe_3$)$_2$-2,3-$C_2B_4H_4$, that the plumbacarboranes have the closo geometry and that the lead was almost symmetrically bonded to the carborane cage above the C_2B_3 face.[4] Very recently, Jutzi and co-workers have reported that the (cyclopentadienyl)lead(II) compounds form adducts with 2,2′-bipyridine.[5] However, the crystal structures of these complexes are still unknown. To date, it is not known whether these plumbacarboranes would form donor–acceptor complexes with Lewis bases and would exhibit the severe slip distortion of the cage upon complexation as was found for the *closo*-stanna- and germacarboranes.[1e,f] Here we describe, in detail, the preparation, characterization, and properties of *C*-trimethylsilyl-substituted η^5-*closo*-plumbacarboranes (I–III) and their donor–acceptor complexes with 2,2′-bipyridine (IV–VI). In addition, the X-ray crystal structures of *closo*-1-Pb-2,3-($SiMe_3$)$_2$-2,3-$C_2B_4H_4$ (I), *closo*-1-Pb-2-($SiMe_3$)-3-(Me)-2,3-$C_2B_4H_4$ (II), and the donor–acceptor complex 1-Pb($C_{10}H_8N_2$)-2,3-($SiMe_3$)$_2$-2,3-$C_2B_4H_4$ (IV) will be presented in detail.

(1) (a) Grimes, R. N. *Rev. Silicon, Germanium, Tin, Lead Compd.* **1977**, *2*, 223. (b) In *Carboranes*; Academic Press: New York, 1970. (c) In *Comprehensive Organometallic Chemistry*; Wilkinson, G., Stone, F. G. A., Abel, E. W., Eds.; Pergamon Press: Oxford, 1982; Vol. 1, and references therein. (d) Grimes, R. N., Ed. *Metal Interactions with Boron Clusters*; Plenum: New York, 1982. (e) Hosmane, N. S.; Maguire, J. A. In *Advances in Boron and the Boranes*; Vol. 5 in the series *Molecular Structure and Energetics*; Liebman, J. F., Greenberg, A., Williams, R. E., Eds.; VCH: New York, 1988, Chapter 14, p 297. (f) Hosmane, N. S.; Maguire, J. A. *Adv. Organomet. Chem.* **1990**, *30*, 99.

(2) (a) Voorhees, R. L.; Rudolph, R. W. *J. Am. Chem. Soc.* **1969**, *91*, 2173. (b) Rudolph, R. W.; Voorhees, R. L.; Cochoy, R. E. *J. Am. Chem. Soc.* **1970**, *92*, 3351.

(3) Wong, K.-S.; Grimes, R. N. *Inorg. Chem.* **1977**, *16*, 2053.

(4) Hosmane, N. S.; Siriwardane, U.; Zhu, H.; Zhang, G.; Maguire, J. A. *Organometallics* **1989**, *8*, 566.

(5) Jutzi, P.; Dickbreder, R.; Nöth, H. *Chem. Ber.* **1989**, *122*, 865.

0276-7333/90/2309-0808$02.50/0

Experimental Section

Materials. 2,3-Bis(trimethylsilyl)-2,3-dicarba-*nido*-hexaborane(8), 2-(trimethylsilyl)-3-methyl-2,3-dicarba-*nido*-hexaborane(8), and 2-(trimethylsilyl)-2,3-dicarba-*nido*-hexaborane(8) were prepared by the methods of Hosmane et al.[6-8] Solutions of the sodium salts of the *nido*-carborane anions, [2-(SiMe$_3$)-3-R-2,3-$C_2B_4H_5$]$^-$ (R = SiMe$_3$, Me, or H) in THF were prepared by the method of Onak and Dunks.[9] Prior to use, anhydrous lead(II) chloride (Strem Chemicals, Inc., Newburyport, MA) was heated to 150 °C in vacuo for 18 h to remove any last traces of H_2O impurity. Purity was checked by IR and NMR spectra. 2,2′-Bipyridine was obtained from Aldrich Chemical Co., Milwaukee, WI, and was sublimed in vacuo before use. NaH (Aldrich) in mineral oil dispersion was washed repeatedly with dry pentane. Tetrahydrofuran (THF) and benzene were dried over $LiAlH_4$ and doubly distilled before use. Acetonitrile (CH_3CN) was dried and stored over CaH_2 and distilled before use. All other solvents were dried over 4–8 mesh molecular sieves (Davidson) and either saturated with dry argon or degassed before use.

Spectroscopic Procedures. Proton, boron-11, and carbon-13 pulse Fourier transform NMR spectra, at 200, 64.2, and 50.3 MHz, respectively, were recorded on an IBM-200 SY multinuclear NMR spectrometer. Electron-impact (EI) mass spectral data were obtained on a Hewlett-Packard GC/MS System 5988A, and the chemical ionization (CI) mass spectral data were obtained from Oneida Research Services, Inc., Whitesboro, NY. Infrared spectra were recorded on a Perkin-Elmer Model 283 infrared spectrometer and a Perkin-Elmer Model 1600 FT-IR spectrophotometer.

Synthetic Procedures. All experiments were carried out in Pyrex glass round-bottom flasks of 250-mL capacity, containing magnetic stirring bars and fitted with high-vacuum Teflon valves. Nonvolatile substances were manipulated in a drybox (Vacuum Atmosphere) under an atmosphere of dry nitrogen. All known compounds among the products were identified by comparing their infrared and ^1H NMR spectra with those of authentic samples.

Synthesis of *closo*-1-Pb^{II}-2-(SiMe$_3$)-3-(R)-2,3-$C_2B_4H_4$ (R = SiMe$_3$, Me, and H). In a procedure identical with that employed in the synthesis of *closo*-stannacarborane,[10] 1.70 (7.74 mmol), 1.35 (8.36 mmol), or 2.06 g (13.97 mmol) *nido*-2-(SiMe$_3$)-3-(R)-2,3-$C_2B_4H_6$ in tetrahydrofuran (THF, 30 mL) was reacted with an excess quantity of NaH [0.21 g, 8.75 mmol; 0.25 g, 10.42 mmol; or 0.37 g, 15.42 mmol when R = SiMe$_3$, Me, or H) in THF to produce Na$^+$[2-(SiMe$_3$)-3-(R)-2,3-$C_2B_4H_5$]$^-$, which was then allowed to react with anhydrous $PbCl_2$ (2.16 g, 7.77 mmol; 2.35 g, 8.45 mmol; or 3.92 g, 14.09 mmol) in THF at −23 °C with constant stirring for 3 h. After removal of THF at this temperature in vacuo, the reaction flask was attached to a series of detachable U-traps. Upon vacuum sublimation of the dark-brown residue at 150 °C, 0.83 g (1.95 mmol, 25% yield) of off-white solid, identified as 1-Pb-2,3-(SiMe$_3$)$_2$-2,3-$C_2B_4H_4$ (I), 1.13 g (3.08 mmol, 37% yield) of off-white solid, identified as 1-Pb-2-(SiMe$_3$)-3-(Me)-2,3-$C_2B_4H_4$ (II), or 1.32 g (3.74 mmol, 27% yield) of grayish white solid, identified as 1-Pb-2-(SiMe$_3$)-2,3-$C_2B_4H_5$ (III), was collected in a trap held at 0 °C, while the neutral *nido*-carborane precursor 2-(SiMe$_3$)-3-(R)-2,3-$C_2B_4H_6$ (0.53 g, 2.41 mmol; 0.47 g, 2.91 mmol; or 0.73 g, 4.95 mmol when R = SiMe$_3$, Me, or H) was collected in a U-trap held at −78 °C. The black residue that remained in the reaction flask (not measured) was identified by qualitative analyses as a mixture of NaCl and elemental lead (Pb^0) and was discarded.

The physical properties and characterization of I are as follows: off-white solid; mp 207–208 °C; sensitive to air and moisture; at 25 °C, reasonably soluble in CH_3CN and THF and slightly soluble in $CHCl_3$, C_6H_6, and C_6H_{14}; ^1H NMR (C_6D_6, relative to external Me_4Si) δ 5.48 [q (v br), 1 H, basal H$_t$, $^1J(^1H-^{11}B)$ = 146 Hz], 5.23 [q (v br), 2 H, basal H$_t$, $^1J(^1H-^{11}B)$ = 145 Hz], 3.56 [q (v br), 1 H, apical H$_t$, $^1J(^1H-^{11}B)$ = 160 Hz], 0.40 [s, 18 H, Me$_3$Si]; ^{11}B NMR (C_6D_6, relative to external $BF_3\cdot OEt_2$) δ 37.01 [d (br), 1 B, basal BH, $^1J(^{11}B-^1H)$ = 145.6 Hz], 30.25 [d (br), 2 B, basal BH, $^1J(^{11}B-^1H)$ = 145 Hz], 2.11 [d (br), 1 B, apical BH, $^1J(^{11}B-^1H)$ = 158.5 Hz]; ^{13}C NMR (C_6D_6, relative to external Me_4Si) δ 130.62 [s (br), cage carbons], 2.49 [q, Me$_3$Si, $^1J(^{13}C-^1H)$ = 125.4 Hz]. The IR and mass spectral data of I and their assignments are summarized in Tables 1 and 2 in the supplementary material.

The physical properties and characterization of II are as follows: off-white solid, mp 115–116 °C; sensitive to air and moisture, at 25 °C, reasonably soluble in THF and CH_3CN and slightly soluble in C_6H_6, $CHCl_3$, CH_2Cl_2, and C_6H_{14}; ^1H NMR (C_6D_6, relative to external Me_4Si) δ 4.99 [q (v br), 1 H, basal H$_t$, $^1J(^1H-^{11}B)$ = 141 Hz], 4.18 [q (br, overlapping) 2 H, basal H$_t$, $^1J(^1H-^{11}B)$ = 148 Hz], 3.39 [q (v br), 1 H, apical H$_t$, $^1J(^1H-^{11}B)$ = 163 Hz], 2.76 [s, 3H, $C_{cage}-CH_3$], 0.32 [s, 9H, Me$_3$Si]; ^{11}B NMR (C_6D_6, relative to external $BF_3\cdot OEt_2$) δ 38.04 [d (br), 1B, basal BH, $^1J(^{11}B-^1H)$ = 140.6 Hz], 28.09 [d (br), 1 B, basal BH, $^1J(^{11}B-^1H)$ = 147.0 Hz], 26.11 [d (br), 1 B, basal BH, $^1J(^{11}B-^1H)$ = 147.5 Hz]; 5.10 [d (br), 1 B, apical BH, $^1J(^{11}B-^1H)$ = 162.7 Hz]; ^{13}C NMR ($CDCl_3$, relative to external Me_4Si) δ 128.0 [s (br), cage carbon (SiCB)], 124.5 [s (br), cage carbon (CCB)], 22.83 [q, $C_{cage}-CH_3$, $^1J(^{13}C-^1H)$ = 128 Hz], 0.83 [q (br), Me$_3$Si, ^1J ($^{13}C-^1H$) = 119.5 Hz]. The IR and mass spectral data of II and their assignments are summarized in Tables 1 and 2 of the supplementary material.

The physical properties and characterization of III are as follows: off-white solid, mp 134–135 °C; sensitive to air and moisture; at 25 °C, reasonably soluble in THF and CH_3CN, slightly soluble in C_6H_6, $CHCl_3$, and CH_2Cl_2, and sparingly soluble in C_6H_{14} and C_6H_{12}; ^1H NMR (CD_3CN, relative to external Me_4Si) δ 6.57 [s (br), 1 H, cage CH], 5.69 [q (v br), 1 H, basal H$_t$, $^1J(^1H-^{11}B)$ = 137 Hz], 4.64 [q (v br), 1 H, basal H$_t$, $^1J(^1H-^{11}B)$ = 153 Hz], 4.47 [q (v br), 1 H, basal H$_t$, $^1J(^1H-^{11}B)$ = 149 Hz], 3.82 [q (v br), 1 H, apical H$_t$, $^1J(^1H-^{11}B)$ = 164 Hz], 0.24 [s, 9 H, Me$_3$Si]; ^{11}B NMR (CD_3CN, relative to external $BF_3\cdot OEt_2$) δ 42.76 [d (br), 1 B, basal BH, $^1J(^{11}B-^1H)$ = 136.6 Hz], 30.77 [d (br), 1 B, basal BH, $^1J(^{11}B-^1H)$ = 153.8 Hz], 28.30 [d (br), 1 B, basal BH, $^1J(^{11}B-^1H)$ = 148.3 Hz], 6.33 [d (br), 1 B, apical BH, $^1J(^{11}B-^1H)$ = 164.1 Hz]; ^{13}C NMR (CD_3CN, relative to external Me_4Si) δ 122.09 [s (br), cage carbon (SiCB)], 110.39 [d (br), cage CH, $^1J(^{13}C-^1H)$ = 154 Hz], −0.40 [q (br), Me$_3$Si, $^1J(^{13}C-^1H)$ = 120 Hz]. The IR and mass spectral data of III and their assignments are summarized in Tables 1 and 2 of the supplementary material.

Synthesis of 1-Pb(C$_{10}$H$_8$N$_2$)-2-(SiMe$_3$)-3-(R)-2,3-$C_2B_4H_4$ (R = SiMe$_3$, Me, and H). An acetonitrile (CH_3CN) or benzene (C_6H_6) solution (10–15 mL) of anhydrous 2,2′-bipyridine, $C_{10}H_8N_2$ (0.15 g, 0.95 mmol; 0.622 g, 3.98 mmol; or 0.26 g, 1.67 mmol) was poured in vacuo into a reaction flask equipped with a magnetic stirring bar and containing 1-Pb-2,3-(SiMe$_3$)$_2$-2,3-$C_2B_4H_4$ (I, 0.40 g, 0.94 mmol), 1-Pb-2-(SiMe$_3$)-3-(Me)-2,3-$C_2B_4H_4$ (II, 1.46 g, 3.98 mmol), or 1-Pb-2-(SiMe$_3$)-2,3-$C_2B_4H_5$ (III, 0.59 g, 1.67 mmol) at −78 °C. When the reaction flask was placed in an ice bath, no color was developed to the solution. This solution was constantly stirred for 2 h at 0 °C and then at room temperature for 3 days, during which time the solution turned gradually from a clear pale yellow to turbid pale orange and no gas evolution was detected. The boron-11 NMR spectra of this solution indicated that the reaction was complete. The solvent, CH_3CN or C_6H_6, was then removed slowly by pumping the reaction mixture at 25 °C. The yellow/grey residue in the reaction flask was washed in vacuo repeatedly with dry *n*-hexane (~10 mL) to remove any last traces of unreacted 2,2′-bipyridine (not measured). The washed residue was then heated to 140–150 °C in vacuo, pumped through a detachable U-trap, and held at 0 °C over 18 h to collect the yellow crystalline solid 1-Pb-(C$_{10}$H$_8$N$_2$)-2,3-(SiMe$_3$)$_2$-2,3-$C_2B_4H_4$ (IV, 0.46 g, 0.79 mmol; 84% yield), the pale orange solid 1-Pb-(C$_{10}$H$_8$N$_2$)-2-(SiMe$_3$)-3-(Me)-2,3-$C_2B_4H_4$ (V, 1.26 g, 2.41 mmol; 61% yield), or the yellow/red solid 1-Pb(C$_{10}$H$_8$N$_2$)-2-(SiMe$_3$)-2,3-$C_2B_4H_5$ (VI, 0.58 g, 1.14 mmol; 68% yield) on the inside walls of the U-trap. The side arms of both the reaction flask and the U-trap were maintained at 140–150 °C with heating tape during the sublimation. The decomposition products, elemental lead (Pb^0) and 2,2′-bipyridine, were not detected among the sublimate.

The physical properties and characterization of IV are as follows: mp 157–158 °C; sensitive to air and moisture; at room temperature, slightly soluble in CH_3CN, THF, C_6D_6, CCl_4, CH_2Cl_2,

(6) Hosmane, N. S.; Sirmokadam, N. N.; Mollenhauer, M. N. *J. Organomet. Chem.* **1985**, *279*, 359.
(7) Hosmane, N. S.; Mollenhauer, M. N.; Cowley, A. H.; Norman, N. C. *Organometallics* **1985**, *4*, 1194.
(8) Hosmane, N. S.; Maldar, N. N.; Potts, S. B.; Rankin, D. W. H.; Robertson, H. E. *Inorg. Chem.* **1986**, *25*, 1561.
(9) Onak, T.; Dunks, G. B. *Inorg. Chem.* **1966**, *5*, 439.
(10) Hosmane, N. S.; Sirmokadam, N. N.; Herber, R. H. *Organometallics* **1984**, *3*, 1665.

and $CDCl_3$, solubility increases at higher temperature without decomposition; ^1H NMR (d_8-THF, relative to external Me_4Si) δ 8.47 [d, 2 H, bpy ring, $^3J(^1H-^1H)$ = 4.5 Hz], 8.23 [d, 2 H, bpy ring, $^3J(^1H-^1H)$ = 8.8 Hz], 7.70 [t, 2 H, bpy ring, $^3J(^1H-^1H)$ = 8.8 Hz], 7.24 [t, 2 H, bpy ring, $^3J(^1H-^1H)$ = 4.5 Hz], 4.77 [q (br), 1 H, basal H_t, $^1J(^1H-^{11}B)$ = 110 Hz], 3.89 [q (br), 2 H, basal H_t, $^1J(^1H-^{11}B)$ = 108 Hz], 1.95 [q (br), 1 H, apical H_t, $^1J(^1H-^{11}B)$ = 144 Hz], 0.45 [s, 18 H, Me_3Si]; ^{11}B NMR (d_8-THF, relative to external $BF_3{\cdot}OEt_2$) δ 39.57 [d, 1 B, basal BH, $^1J(^{11}B-^1H)$ = 110 Hz], 31.93 [d, 2 B, basal BH, $^1J(^{11}B-^1H)$ = 108 Hz], −2.61 [d, 1 B, apical BH, $^1J(^{11}B-^1H)$ = 145 Hz]; ^{13}C NMR (d_8-THF, relative to external Me_4Si) δ 156.31 [s, 2,2′-C, bpy ring], 149.84 [d, bpy ring, $^1J(^{13}C-^1H)$ = 178.5 Hz], 137.98 [d, bpy ring, $^1J(^{13}C-^1H)$ = 162.4 Hz], 126.86 [s (br), cage carbon (SiCB)], 124.95 [d, bpy ring, $^1J(^{13}C-^1H)$ = 156.5 Hz], 121.93 [d, bpy ring, $^1J(^{13}C-^1H)$ = 160.5 Hz], 2.98 [q, 6C, Me_3Si, $^1J(^{13}C-^1H)$ = 119 Hz]. The IR spectral data of IV are summarized in Table 1 of the supplementary material. Both the EI and CI mass spectra of IV do not exhibit the parent ion grouping (see supplementary material, Table 2).

The physical properties and characterization of V are as follows: mp 153–154 °C; sensitive to air and moisture; at room temperature, slightly soluble in CH_3CN, THF, C_6D_6, CCl_4, CH_2Cl_2, and $CDCl_3$, solubility increases at higher temperature without decomposition; ^1H NMR ($CDCl_3$, relative to external Me_4Si) δ 8.68 [d, 2 H, bpy ring, $^3J(^1H-^1H)$ = 4.7 Hz], 8.29 [d, 2 H, bpy ring, $^3J(^1H-^1H)$ = 7.8 Hz], 7.80 [t, 2 H, bpy ring, $^3J(^1H-^1H)$ = 7.8 Hz], 7.30 [t, 2 H, bpy ring, $^3J(^1H-^1H)$ = 5.2 Hz], 4.41 [q (br), 1 H, basal H_t, $^1J(^1H-^{11}B)$ = 130 Hz], 3.53 [q (br), 2 H, basal H_t, $^1J(^1H-^{11}B)$ = 126 Hz], 2.61 [s, 3 H, C_{cage}–Me], 2.09 [q (br), 1 H, apical H_t, $^1J(^1H-^{11}B)$ = 158 Hz], 0.34 [s, 9 H, Me_3Si]; ^{11}B NMR ($CDCl_3$, relative to external $BF_3{\cdot}OEt_2$) δ 33.6 [d, 1 B, basal BH, $^1J(^{11}B-^1H)$ = 134 Hz], 22.5 [d (br), 2 B, basal BH, $^1J(^{11}B-^1H)$, = 126 Hz], −8.22 [d, 1 B, apical BH, $^1J(^{11}B-^1H)$ = 157 Hz]; ^{13}C NMR ($CDCl_3$, relative to external Me_4Si) δ 153.63 [s, 2,2′-C, bpy ring], 148.77 [d, bpy ring, $^1J(^{13}C-^1H)$ = 180 Hz], 138.08 [d, bpy ring, $^1J(^{13}C-^1H)$ = 164.4 Hz], 125.96 [s (br), cage carbon (SiCB)], 124.83 [d, bpy ring, $^1J(^{13}C-^1H)$ = 165.3 Hz], 121.84 [d, bpy ring, $^1J(^{13}C-^1H)$ = 163.8 Hz], 120.62 [s (br), cage carbon (CCB)], 23.04 [q, 1 C, Me, $^1J(^{13}C-^1H)$ = 127.7 Hz], 1.16 [q, 3C, Me_3Si, $^1J(^{13}C-^1H)$ = 119 Hz]. The IR spectral data of V are summarized in the supplementary material, Table 1. The CI mass spectrum of V exhibits the parent ion grouping (see supplementary material, Table 2).

The physical properties and characterization of VI are as follows: mp 127–128 °C; sensitive to air and moisture; at room temperature, reasonably soluble in CH_3CN, THF, C_6D_6, CCl_4, CH_2Cl_2, and $CDCl_3$, solubility increases at higher temperature without decomposition; ^1H NMR (CD_3CN, relative to external Me_4Si) δ 8.70 [d, 2 H, bpy ring, $^3J(^1H-^1H)$ = 4.9 Hz], 8.30 [d, 2 H, bpy ring, $^3J(^1H-^1H)$ = 8.0 Hz], 7.83 [t, 2 H, bpy ring, $^3J(^1H-^1H)$ = 7.8 Hz], 7.34 [t, 2 H, bpy ring, $^3J(^1H-^1H)$ = 5.1 Hz], 6.57 [s (br), 1 H, C_{cage}–H], 4.86 [q (br), 1 H, basal H_t, $^1J(^1H-^{11}B)$ = 120 Hz], 4.1 [q (br, overlapping), 2 H, basal H_t, $^1J(^1H-^{11}B)$ = 126 Hz], 2.10 [q (br), 1 H, apical H_t, $^1J(^1H-^{11}B)$ = 157 Hz], 0.27 [s, 9 H, Me_3Si]; ^{11}B NMR (CD_3CN, relative to external $BF_3{\cdot}OEt_2$) δ 39.5 [d, 1 B, basal BH, $^1J(^{11}B-^1H)$ = 121 Hz], 26.96 [d, 1 B, basal BH, $^1J(^{11}B-^1H)$ = 127 Hz], 25.78 [d, 1 B, basal BH, $^1J(^{11}B-^1H)$ = 125 Hz], −9.78 [d, 1 B, apical BH, $^1J(^{11}B-^1H)$ = 157 Hz]; ^{13}C NMR (CD_3CN, relative to external Me_4Si) δ 155.1 [s, 2,2′-C, bpy ring], 149.8 [d, bpy ring, $^1J(^{13}C-^1H)$ = 180.8 Hz], 139.8 [d, bpy ring, $^1J(^{13}C-^1H)$ = 160.2 Hz], 124.03 [d, bpy ring, $^1J(^{13}C-^1H)$ = 168.2 Hz], 123.78 [s (br), cage carbon (SiCB)], 121.27 [d, bpy ring, $^1J(^{13}C-^1H)$ = 159.1 Hz], 108.8 [d (br), C_{cage}–H, $^1J(^{13}C-^1H)$ = 156 Hz], 0.21 [q, 3 C, Me_3Si, $^1J(^{13}C-^1H)$ = 120 Hz]. The IR spectral data of VI are summarized in the supplementary material, Table 1.

X-ray Analyses of *closo*-1-Pb-2,3-$(SiMe_3)_2$-2,3-$C_2B_4H_4$ (I), *closo*-1-Pb-2-$(SiMe_3)$-3-(Me)-2,3-$C_2B_4H_4$ (II), and 1-Pb-$(C_{10}H_8N_2)$-2,3-$(SiMe_3)_2$-2,3-$C_2B_4H_4$ (IV). Suitable off-white needle-shaped crystals of I and pale yellow crystals of its donor–acceptor complex (IV) were grown very slowly in benzene solutions, while off-white crystals of II were sublimed in vacuo onto a glass surface. Since the crystals all turned opaque white even upon brief exposure to air and/or moisture, compounds I and II were coated with an epoxy resin and the crystals of IV were introduced in 0.5-mm capillary tubes in drybox and sealed. Data for I, II, and IV were collected on an automatic Nicolet R3m/V diffractometer with Mo Kα radiation at 233, 253, and 213 K, respectively. The pertinent crystallographic data are summarized in Table I. Three standard reflections were remeasured after every 100 reflections during the data collection. These data were corrected for decay, for Lorentz–polarization effects, and for absorption (based on Ψ scans). The structures were solved by SHELXTL-PLUS[11] and subsequent difference Fourier maps. All hydrogen atoms were placed in calculated positions with fixed isotropic temperature factors. Final full-matrix least-squares refinements were carried out using the SHELXTL-PLUS system of programs.[11] The function minimized was $\sum\omega(|F_o| - |F_c|)^2$. All non-hydrogen atoms of I, II, and IV were refined anisotropically. Since the anisotropic refinement of atom B(26) of II reached a positively undefined value, isotropic refinement was carried out for this particular atom. In the final stages of refinement a weighting scheme was used (see Table I). Scattering factors used for all atoms as well as the real and imaginary parts of the dispersion correction for Pb and Si were those stored in SHELXTL-PLUS. The final atomic coordinates are given in Table II. Selected bond lengths and bond angles are presented in Table III.

Table I. Crystallographic Data[a] for I, II, and IV

	I	II	IV
formula	$C_8H_{22}B_4Si_2Pb{\cdot}0.5C_6H_6$	$C_{12}H_{32}B_8Si_2Pb_2$	$C_{18}H_{30}B_4N_2Si_2Pb$
fw	463.9	733.4	581.0
cryst system	triclinic	triclinic	monoclinic
space group	$P\bar{1}$	$P\bar{1}$	$P2_1/n$
a, Å	6.409 (6)	6.343 (2)	6.966 (4)
b, Å	10.068 (11)	12.286 (5)	35.49 (3)
c, Å	14.86 (2)	16.593 (6)	9.762 (8)
α, deg	79.5 (1)	73.33 (3)	
β, deg	88.3 (1)	82.45 (3)	102.30 (6)
γ, deg	74.13 (9)	80.08 (3)	
U, Å^3	907 (2)	1215.5 (8)	2358 (3)
Z	2	2	4
D_{calcd}, g cm^{-3}	1.70	2.37	1.64
cryst dmns, mm	0.10 × 0.20 × 0.40	0.10 × 0.20 × 0.10	0.20 × 0.20 × 0.30
scan type	$\theta/2\theta$	$\theta/2\theta$	$\theta/2\theta$
scan sp in ω; min, max	3.0–15.0	3.0–15.0	3.0–15.0
2θ range	3.0, 45.0	3.0, 45.0	3.0, 45.0
data collected	2482	2379	3311
T, K	233	253	213
decay, %	16.00	1.45	10.84
unique data	2370	2273	3049
obsd reflctns, I > 3.0σ(I)	2077	1789	2414
R^b	0.048	0.038	0.034
R_w	0.050	0.053	0.040
$\Delta\rho$(max, min), e/Å^3	2.14 (close to Pb), −2.18	1.48 (close to Pb), −1.83	1.34 (close to Pb), −1.21
k^c	0.0054	0.0035	0.00024

[a] Graphite-monochromatized Mo Kα radiation, λ = 0.710 73 Å. [b] $R = \sum||F_o| - |F_c||/\sum|F_o|$, $R_w = [\sum\omega(F_o - F_c)^2/\sum\omega(F_o)^2]^{1/2}$. [c] $\omega = 1/[\sigma^2(F_o) + k(F_o)^2]$.

Results and Discussion

Synthesis. The *closo*-plumbacarboranes 1-Pb-2,3-$(SiMe_3)_2$-2,3-$C_2B_4H_4$ (I), 1-Pb-2-$(SiMe_3)$-3-(Me)-2,3-$C_2B_4H_4$ (II), and 1-Pb-2-$(SiMe_3)$-2,3-$C_2B_4H_5$ (III) were synthesized in 25–37% yields from their corresponding monosodium salts of the carborane monoanion at −23 °C in THF as shown in Scheme I. When the reaction temperature was increased to 25 °C, the yields were much lower; elemental lead (Pb^0) and the *nido*-carborane precursor were produced predominantly. Therefore, it was essential to carry out the reactions in Scheme I at −23 °C and to pump out the solvent, THF, at this temperature (see Experimental Section). Since under conditions similar to those shown in Scheme I, the sodium/lithium or dilithium double salts

(11) Sheldrick, G. M. *Structure Determination Software Programs*; Nicolet Instrument Corp., USA, 1988.

Table II. Atomic Coordinates (×10⁴) and Equivalent Isotropic Displacement Coefficients (10³Å²) for I, II, and IV

	x	y	z	U(eq)[a]
		I		
Pb	4001 (1)	3401 (1)	5838 (1)	35 (1)
Si(1)	3698 (6)	5607 (4)	7882 (3)	37 (1)
Si(2)	6396 (6)	1540 (4)	8487 (3)	37 (1)
C(1)	5213 (23)	4332 (16)	7186 (10)	37 (5)
C(2)	6313 (21)	2775 (13)	7368 (9)	30 (5)
B(3)	7858 (27)	2264 (17)	6569 (11)	36 (6)
B(4)	7838 (23)	3758 (18)	5816 (10)	32 (6)
B(5)	6040 (26)	5036 (18)	6238 (10)	33 (6)
B(6)	8091 (24)	3776 (18)	6941 (11)	33 (6)
C(3)	5643 (35)	6548 (20)	8246 (14)	74 (9)
C(4)	2238 (37)	4916 (21)	8892 (12)	77 (9)
C(5)	1315 (30)	6802 (19)	7093 (13)	63 (7)
C(6)	8372 (26)	-178 (17)	8423 (12)	55 (6)
C(8)	7434 (22)	2211 (19)	9441 (11)	48 (6)
C(7)	3717 (42)	1293 (23)	8692 (15)	93 (11)
C(9)	3769 (43)	-160 (22)	5754 (17)	78 (10)
C(10)	6176 (49)	-704 (21)	5773 (17)	91 (12)
C(11)	7155 (28)	-500 (26)	4973 (20)	75 (10)
		II		
Pb(1)	3257 (1)	7367 (1)	6677 (1)	43 (1)
Si(1)	698 (8)	7638 (5)	9085 (3)	43 (2)
C(11)	420 (23)	7752 (15)	7955 (10)	34 (7)
C(12)	-314 (25)	6890 (14)	7628 (11)	35 (7)
B(13)	-717 (30)	7309 (20)	6689 (13)	39 (10)
B(14)	-196 (33)	8657 (18)	6355 (13)	36 (9)
B(15)	658 (32)	8875 (17)	7232 (12)	33 (9)
B(16)	-1689 (31)	8263 (18)	7311 (13)	37 (9)
C(13)	-940 (30)	5797 (16)	8226 (13)	65 (10)
C(14)	2682 (31)	6320 (18)	9503 (14)	79 (11)
C(15)	-1965 (29)	7567 (20)	9727 (12)	78 (12)
C(16)	1798 (33)	8904 (18)	9149 (13)	70 (10)
Pb(2)	276 (1)	8337 (1)	4388 (1)	40 (1)
Si(2)	3221 (8)	7514 (5)	2232 (3)	40 (2)
C(21)	3196 (23)	7477 (13)	3361 (10)	24 (7)
C(22)	2656 (24)	6498 (14)	4104 (10)	30 (7)
B(23)	3137 (32)	6622 (18)	4960 (15)	41 (10)
B(24)	4127 (32)	7882 (20)	4714 (15)	45 (10)
B(25)	4039 (31)	8425 (19)	3661 (12)	38 (9)
B(26)	5087 (31)	6953 (17)	4085 (12)	34 (5)
C(23)	2139 (27)	5400 (15)	4001 (12)	46 (8)
C(24)	4058 (29)	8891 (16)	1564 (12)	54 (9)
C(25)	5034 (28)	6290 (16)	1975 (12)	51 (9)
C(26)	360 (26)	7482 (20)	2036 (13)	66 (11)
		IV		
Pb	5163 (1)	1053 (1)	2396 (1)	33 (1)
Si(1)	9567 (5)	1766 (1)	1508 (3)	36 (1)
Si(2)	8510 (4)	1838 (1)	5228 (3)	29 (1)
N(1)	4160 (13)	762 (3)	-181 (10)	37 (4)
N(2)	3633 (13)	388 (3)	2067 (9)	32 (4)
C(1)	8685 (15)	1392 (3)	2583 (11)	24 (4)
C(2)	8375 (15)	1423 (3)	4028 (10)	24 (4)
B(3)	8063 (19)	1025 (4)	4636 (14)	34 (5)
B(4)	8290 (19)	713 (4)	3431 (14)	35 (5)
B(5)	8633 (20)	962 (4)	2082 (15)	33 (5)
B(6)	10000 (20)	1070 (4)	3778 (13)	35 (5)
C(3)	4377 (18)	985 (3)	-1270 (13)	42 (5)
C(4)	3597 (19)	880 (4)	-2646 (13)	49 (5)
C(5)	2639 (17)	542 (4)	-2895 (13)	46 (5)
C(6)	2511 (15)	319 (4)	-1793 (12)	36 (5)
C(7)	3274 (14)	439 (3)	-411 (11)	29 (4)
C(8)	3097 (14)	220 (3)	820 (11)	33 (4)
C(9)	2356 (15)	-154 (3)	729 (13)	36 (4)
C(10)	2174 (16)	-330 (4)	1926 (16)	48 (6)
C(11)	2729 (16)	-165 (4)	3219 (15)	43 (5)
C(12)	3440 (16)	203 (4)	3226 (12)	46 (5)
C(13)	7417 (20)	2078 (4)	704 (13)	61 (6)
C(14)	10386 (19)	1545 (4)	5 (12)	54 (6)
C(15)	11668 (18)	2041 (4)	2547 (13)	51 (5)
C(16)	6711 (18)	1751 (4)	6372 (13)	50 (5)
C(17)	7716 (18)	2291 (3)	4303 (13)	49 (5)
C(18)	11045 (16)	1877 (4)	6356 (12)	45 (5)

[a] Equivalent isotropic U defined as one-third of the trace of the orthogonalized U_{ij} tensor.

Scheme I

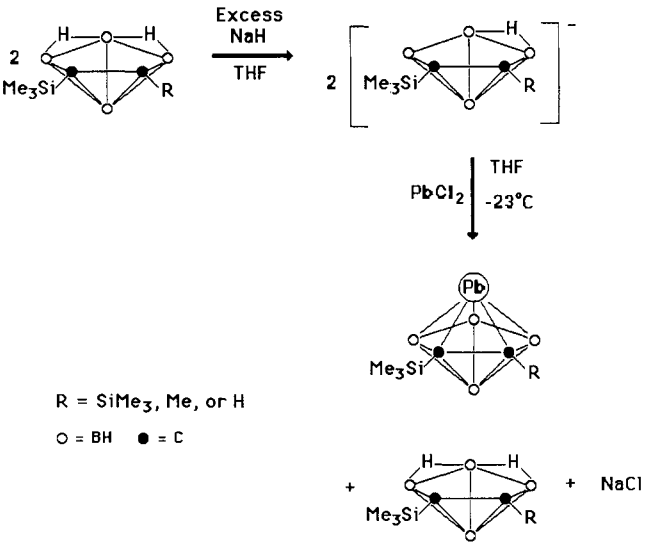

of the *nido*-carborane precursors have an increased tendency to undergo reductive insertion of a group 14 heteroatom, the monosodium salt of the *nido*-carborane precursor was used preferentially.[12] Even then, a substantial quantity of elemental lead was produced due to the reduction of Pb^{II} to Pb^0 during the synthesis of I, II, and III. Perhaps this side reaction is responsible for the low yields of *closo*-plumbacarboranes in Scheme I.

Unlike the stannacarborane systems,[13-16] the *closo*-plumbacarboranes I, II, and III do not readily form the donor–acceptor complexes, 1-Pb($C_{10}H_8N_2$)-2,3-($SiMe_3$)$_2$-2,3-$C_2B_4H_4$ (IV), 1-Pb($C_{10}H_8N_2$)-2-($SiMe_3$)-3-(Me)-2,3-$C_2B_4H_4$ (V), and 1-Pb($C_{10}H_8N_2$)-2-($SiMe_3$)-2,3-$C_2B_4H_5$ (VI) with 2,2′-bipyridine in either benzene or acetonitrile. In fact, the reaction was complete only after 3 days at room temperature, and the resulting complexes were somewhat unstable (see Experimental Section). The slow formation of IV, V, and VI is consistent with that of a germacarborane system in which complexation between the heterocarborane and Lewis base was kinetically controlled.[12c] Since the plumbacarborane complexes have limited solubilities in most of the organic solvents, they were thoroughly washed in dry *n*-hexane to isolate the complexes free from their precursors. The yields of the complexes after washing and sublimation were 61–84%. Since the complexes IV–VI are all colored from yellow to yellow/red, there may be some degree of charge transfer due to $\eta \rightarrow \pi^*$ transitions as in the donor–acceptor complexes of the *closo*-stannacarboranes[13-16] and *closo*-germacarboranes.[12c]

Characterization. The *closo*-plumbacarboranes I, II, and III and their donor–acceptor complexes IV, V, and VI were characterized on the basis of ^1H, ^{11}B, and ^{13}C pulse Fourier transform NMR, IR, and mass spectroscopy (Ex-

(12) (a) Hosmane, N. S.; de Meester, P.; Siriwardane, U.; Islam, M. S.; Chu, S. S. C. *J. Chem. Soc., Chem. Commun.* **1986**, 1421. (b) Siriwardane, U.; Islam, M. S.; West, T. A.; Hosmane, N. S.; Maguire, J. A.; Cowley, A. H. *J. Am. Chem. Soc.* **1987**, *109*, 4600. (c) Hosmane, N. S.; Islam, M. S.; Pinkston, B. S.; Siriwardane, U.; Banewicz, J. J.; Maguire, J. A. *Organometallics* **1988**, *7*, 2340.

(13) Hosmane, N. S.; de Meester, P.; Maldar, N. N.; Potts, S. B.; Chu, S. S. C.; Herber, R. H. *Organometallics* **1986**, *5*, 772.

(14) Siriwardane, U.; Hosmane, N. S.; Chu, S. S. C. *Acta Crystallogr., Sect. C: Cryst. Struct. Commun.* **1987**, *C43*, 1067.

(15) Jutzi, P.; Galow, P.; Abu-Orabi, S.; Arif, A. M.; Cowley, A. H.; Norman, N. C. *Organometallics* **1987**, *6*, 1024.

(16) Siriwardane, U.; Hosmane, N. S. *Acta Crystallogr., Sect. C: Cryst. Struct. Commun.* **1988**, *C44*, 1572.

Table III. Bond Lengths (Å) and Bond Angles (deg) for I, II, and IV

Bond Lengths for I

Pb-C(1)	2.582 (17)	Pb-C(2)	2.634 (14)
Pb-B(3)	2.601 (16)	Pb-B(4)	2.579 (17)
Pb-B(5)	2.520 (20)	Pb(a)-Pb(d)	4.165 (14)
Pb(a)-B(4d)	3.375 (15)	Pb(a)-B(5d)	3.195 (16)
Pb(b)-B(4a)	3.868 (16)	Pb(b)-B(5a)	4.966 (20)
Si(1)-C(1)	1.844 (16)	Si(1)-C(3)	1.901 (25)
Si(1)-C(4)	1.871 (21)	Si(1)-C(5)	1.936 (17)
Si(2)-C(2)	1.879 (13)	Si(2)-C(6)	1.860 (16)
Si(2)-C(8)	1.887 (19)	Si(2)-C(7)	1.810 (28)
C(1)-C(2)	1.510 (19)	C(1)-B(5)	1.601 (21)
C(1)-B(6)	1.821 (20)	C(2)-B(3)	1.590 (21)
C(2)-B(6)	1.751 (23)	B(3)-B(4)	1.700 (23)
B(3)-B(6)	1.755 (27)	B(4)-B(5)	1.678 (22)
B(4)-B(6)	1.688 (23)	B(5)-B(6)	1.766 (20)
C(9)-C(10)	1.488 (39)	C(9)-C(11A)	1.234 (34)
C(10)-C(11)	1.336 (38)	C(11)-C(9A)	1.234 (34)

Bond Lengths for II

Molecule 1

Pb(1)-C(11)	2.690 (16)	Pb(1)-C(12)	2.636 (15)
Pb(1)-B(13)	2.531 (20)	Pb(1)-B(14)	2.494 (19)
Pb(1)-B(15)	2.555 (20)	Pb(1)-B(23)	3.247 (22)
Pb(1)-B(24)	3.128 (22)	Pb(1)-Pb(2)	4.236 (14)
Pb(1b)-B(13a)	3.813 (23)	Si(1)-C(11)	1.869 (19)
Si(1)-C(14)	1.889 (19)	Si(1)-C(15)	1.877 (18)
Si(1)-C(16)	1.845 (25)	C(11)-C(12)	1.483 (29)
C(11)-B(15)	1.562 (23)	C(11)-B(16)	1.740 (26)
C(12)-B(13)	1.536 (27)	C(12)-B(16)	1.729 (24)
C(12)-C(13)	1.504 (24)	B(13)-B(14)	1.666 (32)
B(13)-B(16)	1.760 (34)	B(14)-B(15)	1.721 (34)
B(14)-B(16)	1.723 (28)	B(15)-B(16)	1.754 (31)

Molecule 2

Pb(2)-C(21)	2.641 (16)	Pb(2)-C(22)	2.618 (16)
Pb(2)-B(23)	2.573 (19)	Pb(2)-B(24)	2.505 (21)
Pb(2)-B(25)	2.534 (19)	Pb(2)-B(13)	3.667 (22)
Pb(2)-B(14)	3.368 (23)	Pb(2)-Pb(1)	4.236 (14)
Pb(2a)-B(24b)	3.980 (22)	Si(2)-C(21)	1.858 (18)
Si(2)-C(24)	1.857 (18)	Si(2)-C(25)	1.847 (19)
Si(2)-C(26)	1.895 (19)	C(21)-C(22)	1.505 (20)
C(21)-B(25)	1.583 (31)	C(21)-B(26)	1.722 (25)
C(22)-B(23)	1.546 (32)	C(22)-B(26)	1.723 (27)
C(22)-C(23)	1.501 (27)	B(23)-B(24)	1.692 (33)
B(23)-B(26)	1.778 (27)	B(24)-B(25)	1.687 (29)
B(24)-B(26)	1.743 (34)	B(25)-B(26)	1.785 (27)

Bond Lengths for IV

Pb-N(1)	2.674 (9)	Pb-N(2)	2.581 (9)
Pb-C(1)	2.706 (10)	Pb-C(2)	2.787 (10)
Pb-B(3)	2.643 (12)	Pb-B(4)	2.504 (13)
Pb-B(5)	2.521 (15)	Si(1)-C(1)	1.871 (11)
Si(1)-C(13)	1.891 (14)	Si(1)-C(14)	1.860 (14)
Si(1)-C(15)	1.871 (13)	Si(2)-C(2)	1.874 (11)
Si(2)-C(16)	1.873 (14)	Si(2)-C(17)	1.867 (13)
Si(2)-C(18)	1.877 (11)	N(1)-C(3)	1.357 (17)
N(1)-C(7)	1.299 (15)	N(2)-C(8)	1.338 (14)
N(2)-C(12)	1.339 (16)	C(1)-C(2)	1.477 (15)
C(1)-B(5)	1.603 (17)	C(1)-B(6)	1.744 (16)
C(2)-B(3)	1.563 (18)	C(2)-B(6)	1.739 (18)
B(3)-B(4)	1.650 (21)	B(3)-B(6)	1.740 (21)
B(4)-B(5)	1.642 (21)	B(4)-B(6)	1.724 (20)
B(5)-B(6)	1.769 (18)	C(3)-C(4)	1.389 (17)
C(4)-C(5)	1.371 (20)	C(5)-C(6)	1.350 (18)
C(6)-C(7)	1.408 (15)	C(7)-C(8)	1.455 (16)
C(8)-C(9)	1.422 (17)	C(9)-C(10)	1.352 (20)
C(10)-C(11)	1.372 (20)	C(11)-C(12)	1.397 (19)

Bond Angles for I

C(1)-Pb-C(2)	33.6 (4)	C(1)-Pb-B(3)	60.0 (5)
C(2)-Pb-B(3)	35.4 (5)	C(1)-Pb-B(4)	61.6 (5)
C(2)-Pb-B(4)	60.1 (5)	B(3)-Pb-B(4)	38.3 (5)
C(1)-Pb-B(5)	36.6 (5)	C(2)-Pb-B(5)	59.0 (4)
B(3)-Pb-B(5)	62.9 (5)	B(4)-Pb-B(5)	38.4 (5)
B(4d)-Pb(a)-B(5d)	29.4 (6)	B(4a)-Pb(b)-B(4e)	78.2 (6)
B(4a)-Pb(b)-B(5e)	93.6 (7)	B(5a)-Pb(b)-B(4e)	73.8 (6)
B(5a)-Pb(b)-B(5e)	95.7 (7)	Pb-B(3)-B(4)	70.1 (7)
Pb-B(3)-B(6)	95.6 (8)	Pb-B(4)-B(3)	71.5 (8)
Pb-B(4)-B(5)	68.9 (8)	Pb-B(4)-B(6)	98.1 (9)

Bond Angles for II

Molecule 1

C(11)-Pb(1)-C(12)	32.3 (6)	C(11)-Pb(1)-B(13)	58.0 (7)
C(12)-Pb(1)-B(13)	34.5 (6)	C(11)-Pb(1)-B(14)	60.6 (6)
C(12)-Pb(1)-B(14)	59.8 (5)	B(13)-Pb(1)-B(14)	38.7 (7)
C(11)-Pb(1)-B(15)	34.5 (5)	C(12)-Pb(1)-B(15)	57.6 (6)
B(13)-Pb(1)-B(15)	63.0 (8)	B(14)-Pb(1)-B(15)	39.8 (7)
B(23)-Pb(1)-B(24)	30.7 (10)	B(23)-Pb(1)-B(13)	78.8 (11)
B(23)-Pb(1)-B(14)	88.4 (10)	B(24)-Pb(1)-B(13)	94.6 (11)
B(24)-Pb(1)-B(14)	84.3 (10)		

Molecule 2

C(21)-Pb(2)-C(22)	33.2 (4)	C(21)-Pb(2)-B(23)	58.7 (6)
C(22)-Pb(2)-B(23)	34.6 (7)	C(21)-Pb(2)-B(24)	60.5 (7)
C(22)-Pb(2)-B(24)	60.0 (7)	B(23)-Pb(2)-B(24)	38.9 (7)
C(21)-Pb(2)-B(25)	35.5 (7)	C(22)-Pb(2)-B(25)	59.1 (6)
B(23)-Pb(2)-B(25)	63.6 (6)	B(24)-Pb(2)-B(25)	39.1 (7)
B(13)-Pb(2)-B(14)	27.0 (10)	B(13)-Pb(2)-B(23)	70.5 (11)
B(13)-Pb(2)-B(24)	82.9 (10)	B(14)-Pb(2)-B(23)	84.5 (10)
B(14)-Pb(2)-B(24)	79.2 (11)		

Bond Angles for IV

N(1)-Pb-N(2)	60.6 (3)	N(1)-Pb-C(1)	106.8 (3)
N(2)-Pb-C(1)	139.5 (3)	N(1)-Pb-C(2)	137.7 (3)
N(2)-Pb-C(2)	139.8 (3)	C(1)-Pb-C(2)	31.1 (3)
N(1)-Pb-B(3)	139.9 (4)	N(2)-Pb-B(3)	107.1 (4)
C(1)-Pb-B(3)	55.7 (4)	C(2)-Pb-B(3)	33.3 (4)
N(1)-Pb-B(4)	102.9 (4)	N(2)-Pb-B(4)	85.0 (4)
C(1)-Pb-B(4)	59.2 (4)	C(2)-Pb-B(4)	58.2 (4)
B(3)-Pb-B(4)	37.3 (5)	N(1)-Pb-B(5)	84.3 (4)
N(2)-Pb-B(5)	104.4 (4)	C(1)-Pb-B(5)	35.5 (4)
C(2)-Pb-B(5)	57.0 (4)	B(3)-Pb-B(5)	60.8 (5)
B(4)-Pb-B(5)	38.1 (5)		

perimental Section and Tables 1 and 2 in the supplementary material). The *closo*-plumbacarboranes I and II and the donor–acceptor complex IV were also characterized by single-crystal X-ray diffraction studies (Tables I–IV).

Mass Spectra. Electron-impact (EI) mass spectra were obtained for compounds I and IV, while chemical-ionization (CI) mass spectra were obtained for compounds II, III, and V (see the supplementary material, Table 2). Both the EI and CI mass spectra of the *closo*-plumbacarboranes I, II, and III exhibited the corresponding parent grouping and a weak parent grouping minus a methyl group with

Table IV. Mean Deviations of Least-Squares Planes and Their Dihedral Angles Involving the C_2B_3 Face and 2,2′-Bipyridine Rings in the Donor–Acceptor Complex IV

plane no.	mean dev, Å	plane no.	mean dev, Å
1 [C_2B_3 ring]	0.012	3 [$C_5N(1)$ ring]	0.015
2 [$C_{10}N_2$ ring]	0.071	4 [$C_5N(2)$ ring]	0.005

plane nos.	dihedral angle, deg	plane nos.	dihedral angle, deg
1 and 2	27.5	1 and 4	23.0
1 and 3	32.0	2 and 4	4.6
2 and 3	4.6	3 and 4	9.2

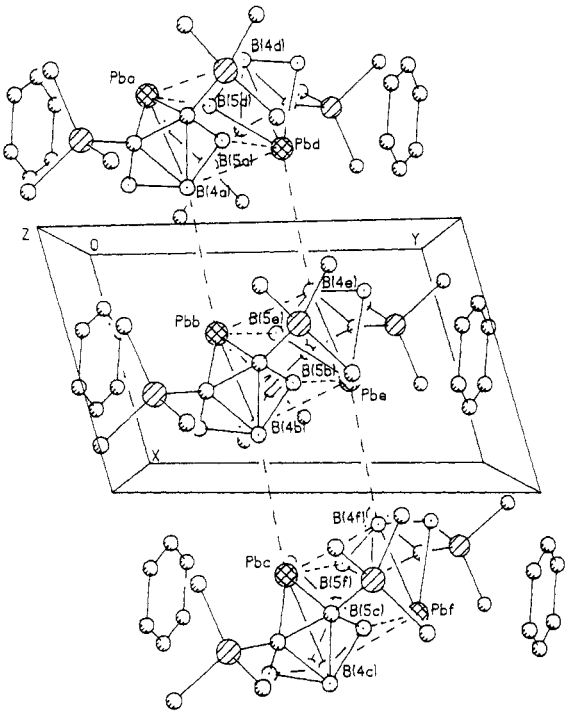

Figure 1. Crystal packing diagram showing the extended network of [*closo*-1-Pb-2,3-$(SiMe_3)_2$-2,3-$C_2B_4H_4$]$_2$ molecular dimers with benzene molecules of crystallization. The dotted lines represent the nonbonded contacts within and between the dimeric clusters.

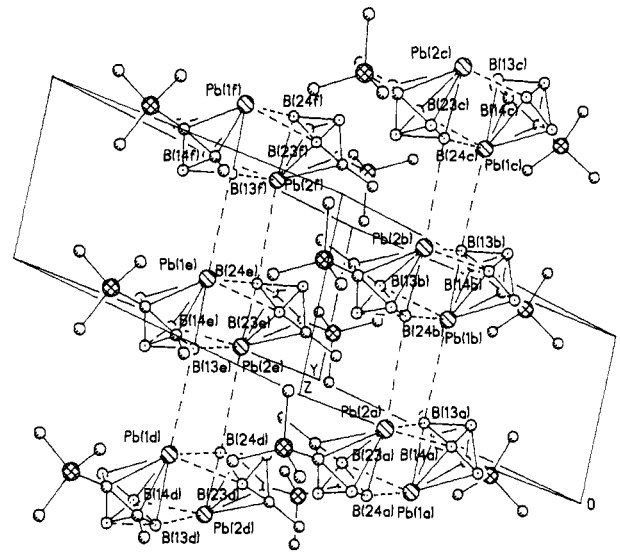

Figure 2. Crystal packing diagram showing two parallel extended networks of [*closo*-1-Pb-2-$(SiMe_3)$-3-(Me)-2,3-$C_2B_4H_4$]$_2$ molecular dimers of two independent molecules with a crystallographic center of inversion between the two parallel networks. The dotted lines represent the nonbonded contacts within and between the dimeric clusters.

the major cutoffs at m/z 426 and 411 for I, 369 and 355 for II, and 355 and 340 for III. In addition to other ion fragments, the strong peaks of Pb^+ ions with the local cutoff at m/z 208 and Me_3Si^+ ion at m/z 73 were observed in the mass spectrum of each of the *closo*-plumbacarboranes. The EI mass spectrum of IV (see the supplementary material, Table 2) does not exhibit the parent ion grouping. In this spectrum, the Lewis base 2,2′-bipyridine ion fragment with ~76% relative intensity and the parent and the daughter (parent minus a methyl unit) groupings of the corresponding plumbacarborane precursor have been observed. This indicates that the Pb–N bonds in IV are weak; consequently, these bonds were broken during the ionization at 70 eV. However, the CI mass spectrum of V exhibited a very strong parent grouping [$^{208}Pb(^{12}C_{10}H_8{}^{14}N_2)^{28}Si(^{12}CH_3)_4{}^{12}C_2{}^{11}B_4H_5{}^+$] with the major cutoff at m/z 525. The most common ion fragments in both the EI mass spectrum of IV and the CI mass spectrum of V were $(^{12}CH_3)_3{}^{28}Si^+$, $^{12}C_{10}H_8{}^{14}N_2{}^+$, $^{208}Pb^+$, and the corresponding *closo*-plumbacarborane precursor ion (parent ion minus a bipyridine ligand) at their respective mass-to-charge ratios.

NMR and IR Spectra. The ^1H NMR and ^{13}C NMR spectra indicate the presence of a C_2B_4 carborane cage and $SiMe_3$ and Me or CH groups in compounds I–VI in addition to the presence of a 2,2′-bipyridine ligand in each of the donor–acceptor complexes IV–VI. The significant downfield shifts of both the apical and basal BH proton resonances from those of the *nido*-carborane precursor in the ^1H NMR spectra of I–VI (see Experimental Section) are indicative of deshielding of these protons due to interactions between the apical Pb and the basal borons and between apical Pb and the apical boron through the basal borons. The ^{11}B NMR spectra of the plumbacarboranes I, II, and III all show a downfield doublet due to a basal BH unit in the region of ~43–37 ppm. In I there is another doublet of two equivalent basal BH units near 30 ppm, while in II and III this is separated into two basal BH doublets of intensities 1:1 at 28 and 26, and 31 and 28 ppm, respectively. In addition, all show a doublet in the region 2–6 ppm that is assigned to an apical BH unit in I–III. On the other hand, the bis(trimethylsilyl)-substituted *closo*-stanna- and germacarboranes all exhibit a single doublet corresponding to their three basal BH units.[10,12c] The distinctive separation of one of the basal BH resonances from the remaining ones has also been observed previously in the ^{11}B NMR spectra of 1-Pb-2,3-$(R)_2$-2,3-$C_2B_4H_4$ (R = Me, H)[3] and $PbC_2B_9H_{11}$.[2] The solid-state structures of I and II show that the *closo*-plumbacarboranes have a strong tendency to form molecular dimers (see Figures 1 and 2). If this dimeric structure exists in solution, it is possible that it could contribute to the unusual splitting of the basal boron resonances in their ^{11}B NMR spectra.

Except for the small upfield shift of the apical BH resonance, presumably due to less interaction with the apical Pb atom, the ^{11}B NMR data of IV, V, and VI bear striking similarities to those of their *closo*-plumbacarborane precursors. However, for V, the two nonequivalent basal BH resonances other than that of unique BH appeared as a broad doublet in its proton-coupled ^{11}B NMR spectrum. This is one of the several cases in the C_2B_4 system where the borons bonded to the unsymmetrical C_{cage} atoms appear as a single resonance in the ^{11}B NMR spectra.[3,6,10] With the exception of a very slight change in the ^{13}C chemical shifts of the coordinated 2,2′-bipyridine molecule, both ^1H and ^{13}C spectral data are identical with those of their precursors and hence do not provide any new information regarding the geometries of IV–VI. However, the unambiguous proof for complexation between the 2,2′-bipyridine and the corresponding plumbacarborane is provided by the single-crystal X-ray analysis of IV (discussed in the following section). The presence of the plumbacarborane cages and the coordinated bipyridine was also substantiated by the infrared spectra of I–VI, (see the supplementary material, Table I).

Crystal Structures of *closo*-1-Pb-2,3-$(SiMe_3)_2$-2,3-$C_2B_4H_4$ (I), *closo*-1-Pb-2-$(SiMe_3)$-3-(Me)-2,3-$C_2B_4H_4$ (II), and 1-Pb$(C_{10}H_8N_2)$-2,3-$(SiMe_3)_2$-2,3-$C_2B_4H_4$ (IV). Figures 1 and 2 show the packing diagrams and unit-cell compositions of I and II, respectively. Figure 1 shows that

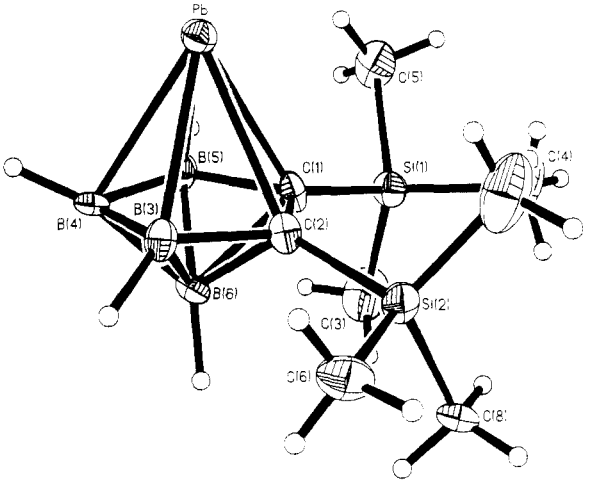

Figure 3. Perspective view of one of the *closo*-plumbacarboranes I in Figure 1 showing the atom numbering scheme and thermal ellipsoids at the 30% probability level.

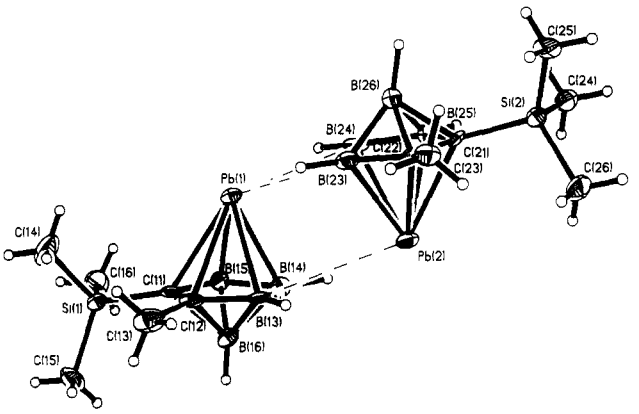

Figure 4. Perspective view of the two crystallographically independent molecules within the dimeric clusters of II in Figure 2 showing the atom numbering scheme and thermal ellipsoids at the 30% probability level.

the unit cell consists of a dimer of two identical *closo*-$Pb(CSiMe_3)_2B_4H_4$ molecules along with one solvated benzene molecule. These are packed in such a way that the solvated benzene molecules can be considered as being intercalated between the layers of an extended dimeric plumbacarborane network. On the other hand, the unit cell of II consists of two [*closo*-$Pb(CSiMe_3)(CMe)B_4H_4]_2$ molecular dimers with a crystallographic center of inversion between the dimers. Each dimer of II consists of two crystallographically independent molecules (labelled as molecules 1 and 2 in Table III). The local geometry of each PbC_2B_4 cage shows that the apical Pb, formally in its +2 oxidation state, is η^5-bonded to the C_2B_3 face of the carborane cage and is located almost directly above the center of this face. The Pb–cage atom distances, in the order C(1), C(2), B(3), B(4), and B(5) (see Figures 3 and 4) are as follows: for compound I, 2.582 (17), 2.634 (14), 2.601 (16), 2.579 (17), and 2.520 (20) Å; for molecule 1 of compound II, 2.690 (16), 2.636 (15), 2.531 (20), 2.494 (19), and 2.555 (20) Å; and for molecule 2 of II, 2.641 (16), 2.618 (16), 2.573 (19), 2.505 (21), and 2.534 (19) Å. If any distortion exists in I, it is one in which the apical Pb atom slipped toward B(5), the basal boron that is bonded to a C_{cage} atom (see Figure 3) rather than toward the unique boron, B(4). However, a slight slippage of the apical Pb toward the unique borons [B(14) and B(24) in Figure 4] is seen in molecules II-1 and II-2. In both I and II the unique boron and the one next to it in the PbC_2B_4 cage are also involved in fairly strong intermolecular dipole–dipole type of interactions between a C_2B_4 group and a neighboring Pb atom within the dimeric cluster (see Figures 1, 2, and 4). For example, Pb(a)–B(5d) and Pb(a)–B(4d) distances in Figure 1 are 3.195 (16) and 3.375 (15) Å, respectively, while Pb(1)–B(24) and Pb(1)–B(23), and Pb(2)–B(13) and Pb(2)–B(14) distances between the two crystallographically independent molecules and within the dimeric cluster unit of II (see Table III and Figure 4) are 3.128 (22) and 3.247 (22) Å, and 3.667 (22) and 3.368 (23) Å, respectively. All structures show that the lead does not reside in the pseudo-mirror plane (the plane containing B(4), B(6), and the midpoint of the C(1)–C(2) bond) of the carborane cage. In all cases the direction of displacement of the apical Pb is toward the other plumbacarborane in the dimeric cluster. This type of distortion would allow for a stronger interaction between the two plumbacarboranes in a dimer. The additional slippage toward the unique boron [B(4)] in II-1 and II-2 is similar in both magnitude and direction to those found in the corresponding stannacarboranes.[1e,f] The intercluster distances of 3.868 (16) Å between Pb(b or d) and B(4a or 4e) in I (see Figure 1), and 3.813 (23) and 3.980 (22) Å between Pb(1b) and B(13a) and between Pb(2a) and B(24b) in II (see Figure 2) exceed the sum of their van der Waals radii,[17] and hence they should not contribute substantially to the distortions of the plumbacarborane cages. MNDO-SCF calculations on the monomeric *closo*-$Pb(SiMe_3)_2C_2B_4H_4$ (I) yielded an optimized geometry in which the apical Pb was in the pseudo-mirror plane of the carborane cage and slightly slipped toward the unique boron indicating that displacement from the mirror plane is probably due to dimer formation (see the supplementary material, Table 6, for optimized bond distances). It is of interest that both theory and experiment show that there is very little change in slip distortion in going from Sn to Pb. Indeed, calculations on the model compounds *closo*-1,2,3-$SnC_2B_4H_6$ and *closo*-1,2,3-$PbC_2B_4H_6$ for a fixed carborane geometry show that the most noticeable change in going from Sn to Pb is that the Sn is bonded above the carborane face by a sharper potential energy profile than is the Pb. The flatter energy surface in the plumbacarboranes is consistent with the multiple structures found for II. The intercluster layers of solvated benzene molecules in I that are not within the van der Waals nonbonded contacts are probably responsible for the differences in crystal packing between I and II. Removal of these intercalated benzene molecules could result in a decrease in the interlayer spacing and consequently, give rise to a packing diagram, similar to the one shown in Figure 2 for II. It is interesting to point out that the shortest Pb–C distance of 2.69 (1) Å in the solid-state structure of the monomeric and slipped $(Me_5C_5)_2Pb$ is considerably longer than even the longest Pb–C_{cage} distances of 2.634 (14) Å in I and 2.641 (16) Å in molecule 2 of II but is comparable to that of molecule 1 of II [2.690 (16) Å].[18] Thus, it is evident that the Pb atoms in the plumbacarborane cages are more covalently bonded than in the plumbocene derivatives.[18]

The X-ray crystal structure of IV, represented in Figure 5, shows that the apical lead is significantly displaced from the centroidal position above the C_2B_3 face and that the 2,2′-bipyridine base is tilted significantly away from the cage carbons with B–Pb–N orientation angles of about 84–140°. The Pb–C_{cage} distances of 2.706 (10) and 2.787

(17) Huheey, J. E. In *Inorganic Chemistry*, 2nd ed.; Harper & Row: New York, 1978; p 232.
(18) Atwood, J. L.; Hunter, W. E.; Cowley, A. H.; Jones, R. A.; Stewart, C. A. *J. Chem. Soc., Chem. Commun.* **1981**, 925.

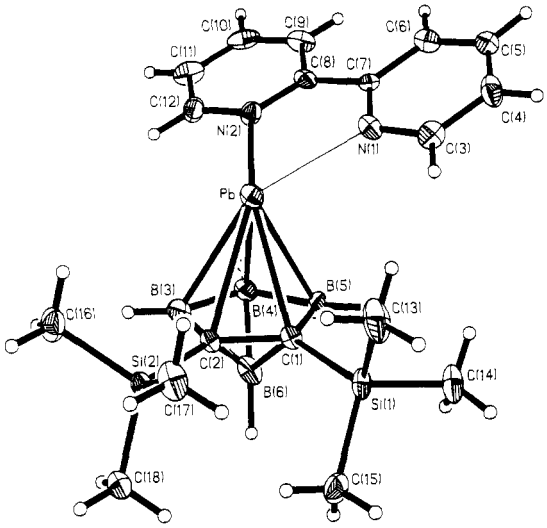

Figure 5. Perspective view of 1-Pb($C_{10}H_8N_2$)-2,3-($SiMe_3$)$_2$-2,3-$C_2B_4H_4$ (IV) with thermal ellipsoids drawn at the 30% probability level and showing the atom numbering scheme. The thinner line represents the weaker interaction between the two atoms.

(10) Å is considerably longer than the Pb–B distances of 2.643 (12), 2.504 (13), and 2.521 (15) Å (see Table III). Surprisingly, one of the Pb–N distances [Pb–N(1) = 2.674 (9) Å] is longer than the other by about 0.1 Å. Consequently, the coordinated 2,2′-bipyridine is not exactly opposite the C–C_{cage} bond; rather, it is twisted toward two of the basal borons [B(4) and B(5) in the C_2B_3 face]. Thus, the apical Pb atom exhibits stronger bonding interactions with one of the nitrogen atoms of the 2,2′-bipyridine [Pb–N(2) = 2.581 (9) Å] and consecutive borons [Pb–B(4) = 2.504 (13) and Pb–B(5) = 2.521 (15) Å] of the carborane cage than with the other similar atoms in IV. It should also be noted that the more strongly bound nitrogen lies almost directly above the unique boron [the N(2)–Pb–B(4)–B(6) torsion angle is 176.7°, while that of N(1)–Pb–B(4)–B(6) is 118.4°]. One of the interesting features of the structure of IV is the overall nonplanarity of the coordinated 2,2′-bipyridine molecule itself with the dihedral angle of 9.2° between its two C_5N rings (see Table IV) when compared to the almost planar alignment found in the stannacarborane–2,2′-bipyridine complex.[13] The dihedral angles between the planes formed by the C_2B_3 face of the plumbacarborane cage and the C_5N rings of the bipyridine ligand containing N(1) and N(2) donor atoms in IV are 32.0 and 23.0°, respectively. However, the dihedral angle of 27.5° between the C_2B_3 face and the calculated overall plane of the 2,2′-bipyridine molecule (see Table IV) is comparable to the dihedral angle of 26.8° in the corresponding stannacarborane complex 1-Sn($C_{10}H_8N_2$)-2,3-($SiMe_3$)$_2$-2,3-$C_2B_4H_4$.[13] Crystal packing of IV (not shown) reveals that the intermolecular interactions within the plumbacarborane dimers are broken upon formation of their donor–acceptor complex with the Lewis base, 2,2′-bipyridine. Structures are now known for the series 1-M-($C_{10}H_8N_2$)-2,3-($SiMe_3$)$_2$-2,3-$C_2B_4H_4$ (M = Ge, Sn, Pb).[12c,13,19]

(19) This work.

Unfortunately, there is no consistent structural pattern to be seen in this series. Although all show that the bipyridine base is generally oriented above the ring borons and that the group 14 metal is significantly slipped toward these borons, there are no discernible trends. While the bipyridine is directly opposite the cage carbons and is symmetrically bonded to the Sn in the stannacarborane system, the corresponding germacarborane and plumbacarborane analogues show unsymmetrical bipyridine bonding. In both complexes one M–N bond is shorter than the other, causing a tilting of the metal-bound base toward the two consecutive borons on the carborane face. Since the 2,2′-bipyridine nitrogens are equivalent and the *closo*-metallacarboranes are almost symmetric with respect to the pseudo-mirror plane of the C_2B_4 cage, there is no apparent reason for the tilting of the bipyridine ligand and the inequality in the M–N and M–B (M = Pb, Ge) bond lengths. MNDO-SCF calculations on the stannacarborane–2,2′-bipyridine complexes[20] showed that when the bipyridine molecule was rotated about the Sn–C_2B_3 axis, the Sn moves toward the direction of rotation and the bipyridine molecule twists so that the leading nitrogen is higher above the tin and at a longer distance than the following one. These are the precise distortions seen in both the germa- and plumbacarboranes. It could be that there is a tendency to form one strong M–N bond, or alternately, crystal packing forces could cause such distortions. Recently, the bipyrimidine complexes of the *closo*-plumbacarboranes have been synthesized, and their structures have been determined.[21] Preliminary X-ray analyses show that the bipyrimidine base is directly opposite the cage carbons as found in the corresponding stannacarborane analogues.[22] Therefore, the symmetric structures for the bipyrimidine complexes is a strong indication that the distortions from the ideal geometry found in the germanium- and lead–bipyridine complexes are more a consequence of lattice packing than an innate bonding preference.

Acknowledgment. This work was supported by grants from the National Science Foundation (CHE-8800328), the Robert A. Welch Foundation (N-1016), and the donors of the Petroleum Research Fund, administered by the American Chemical Society.

Supplementary Material Available: IR absorptions (Table S-1) and mass spectrometric data (Table S-2) of I–VI, anisotropic displacement coefficients of I, II, and IV (Table S-3), selected bond angles and torsion angles of I, II, and IV (Table S-4), H-atom coordinates and isotropic displacement coefficients of I, II, and IV (Table S-5), and optimized bond distances predicted by MNDO-SCF molecular orbital calculations (Table S-6) (24 pages); structure factors of I, II, and IV (Table S-7) (29 pages). Ordering information is given on any current masthead page.

(20) Maguire, J. A.; Ford, G. P.; Hosmane, N. S. *Inorg. Chem.* **1988**, 27, 3354.

(21) Hosmane, N. S.; et al., to be submitted for publication.

(22) (a) Hosmane, N. S.; Islam, M. S.; Siriwardane, U.; Maguire, J. A. *Organometallics* **1987**, *6*, 2447. (b) Hosmane, N. S.; Fagner, J. S.; Zhu, H.; Siriwardane, U.; Maguire, J. A.; Zhang, G.; Pinkston, B. S. *Organometallics* **1989**, *8*, 1769.